Journal of proteome research

pubs.acs.org/jpr

Article

Levetiracetam Treatment Normalizes Levels of Presynaptic Endocytosis Machinery and Restores Nonamyloidogenic APP Processing in *App* Knock-in Mice

Nalini R. Rao and Jeffrey N. Savas*

Cite This: *J. Proteome Res.* 2021, 20, 3580−3589

Read Online

ACCESS | Metrics & More | Article Recommendations | Supporting Information

ABSTRACT: Toxic amyloid-beta (Aβ) peptides, produced by sequential proteolytic cleavage of the amyloid precursor protein (APP), play a key role in the initial stage of Alzheimer's disease (AD). Increasing evidence indicates that Aβ_{42} induces neuronal circuit hyperexcitability in the early stages of AD pathology. As a result, researchers have investigated treatments that modulate the excitatory/inhibitory imbalance as potential AD therapies. For example, levetiracetam, an atypical antiepileptic drug used to quell hyperexcitability, has garnered recent interest in the AD field, even though its exact mechanism(s) of action remains elusive. Here, we show that in APP knock-in mouse models of amyloid pathology, chronic levetiracetam administration decreases cortical Aβ_{42} levels and lowers the amyloid plaque burden. In addition, using multiplexed tandem mass tag-quantitative mass spectrometry-based proteomic analysis, we determined that chronic levetiracetam administration selectively normalizes levels of presynaptic endocytic proteins. Finally, we found that levetiracetam treatment selectively lowers beta carboxyl-terminal fragment levels, while the abundance of full-length APP remains unchanged. In summary, this work reports that chronic treatment with levetiracetam serves as a useful therapeutic in AD by normalizing levels of presynaptic endocytic proteins and altering APP cleavage preference, leading to a decrease in both Aβ_{42} levels and the amyloid plaque burden. These novel findings provide novel evidence for the previously documented therapeutic value of levetiracetam to mitigate AD pathology.

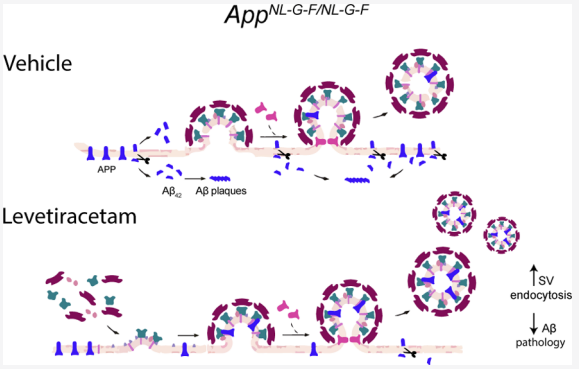

KEYWORDS: *Alzheimer's disease, levetiracetam, APP knock-in, quantitative proteomics, axon terminal, amyloid precursor protein*

INTRODUCTION

In Alzheimer's disease (AD), sequential proteolytic cleavage of the amyloid precursor protein (APP) leads to the production of toxic amyloid-beta (Aβ) peptides. The inability to efficiently degrade Aβ_{42} has been shown to drive downstream pathologies such as synapse deterioration and formation of amyloid plaques and neurofibrillary tangles.[1−4] While downstream repercussions have been documented, there is currently no effective treatment to prevent, reverse, or slow the progression of AD. Notably, Aβ-lowering antibody treatments show promise but have likely been administered too late in the progression of AD.[4] As a result, there has been a shift in focus to identifying and investigating early AD pathologies that may serve as potential therapeutic targets.

Hyperactivity and neural network disruption have been observed during the initial stages of amyloid pathology and could represent a pioneering aspect of AD pathogenesis.[5−7] These findings have motivated recent investigations focused on the role of brain hyperexcitability in AD and subsequently whether modulating the excitatory/inhibitory imbalance could be an efficacious AD therapy. We recently discovered an early impairment in degradation and turnover of synaptic vesicle (SV) machinery in APP knock-in (*App* KI) mouse models of amyloid pathology.[8] Our findings indicate that targeting or correcting early presynaptic proteostasis could represent an effective therapeutic target. Levetiracetam (LEV) is an atypical antiepileptic drug that, unlike those targeting the GABA-ergic system, binds to the presynaptic SV glycoprotein 2A (SV2A).[9] However, despite FDA approval and wide use, levetiracetam's mechanism(s) of actions remain elusive. In APP transgenic mouse models, levetiracetam administration reduces hyperexcitability, suppresses neuronal network dysfunction, and decreases Aβ plaque burden and associated cognitive deficits.[9−13] In a clinical study of patients with mild cognitive impairment, abnormal entorhinal cortex hyperactivity was corrected with chronic levetiracetam administration, and

Received: March 4, 2021
Published: June 9, 2021

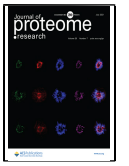

https://doi.org/10.1021/acs.jproteome.1c00180
J. Proteome Res. 2021, 20, 3580−3589

interestingly, these patients simultaneously had an improved working memory performance.[14] Levetiracetam is, to date, the focus of seven phase 1 or 2 clinical trials for AD.[15]

In this study, we set out to identify the pathways and mechanisms primarily affected by levetiracetam in diseased brains of amyloid pathology to determine how levetiracetam affects the proteome. In order to avert the possible confounding effects of APP overexpression, we used *App* KI mouse models that have the humanized Aβ_{42} sequence expressed under the endogenous APP promoter and harbor familial mutations.[16] *App* KI mice harboring the Swedish mutation ($App^{NL/NL}$) serve as controls for mice with an additional Iberian mutation ($App^{NL\text{-}F/NL\text{-}F}$) which increases the ratio of Aβ_{42} to Aβ_{40}, representing a moderate amyloid pathology. Addition of the artic mutation ($App^{NL\text{-}G\text{-}F/NL\text{-}G\text{-}F}$) increases protofibril formation and models severe amyloid pathology.[16] Here, we show that chronic levetiracetam administration decreases cortical Aβ_{42} levels and lowers the amyloid plaque burden. In addition, using multiplexed tandem mass tag (TMT)-quantitative mass spectrometry (MS)-based proteomic analysis, we determined that chronic levetiracetam administration selectively normalizes levels of presynaptic endocytic proteins. Finally, we found that levetiracetam treatment selectively lowers beta carboxyl-terminal fragment (β-CTF) levels, while the abundance of full-length APP remains unchanged. In summary, this work reports that chronic treatment with levetiracetam serves as a useful therapeutic in AD by normalizing levels of presynaptic endocytic proteins and altering APP cleavage preference, leading to a decrease in both Aβ_{42} levels and the amyloid plaque burden. These novel findings provide pioneering evidence for the previously documented therapeutic value of levetiracetam in mitigating AD pathology.

METHODS

Animals

All experiments performed were approved by the Institutional Animal Care and Use Committee of Northwestern University (protocols IS0009900 and IS00010858). The mice used for all experiments were *App* KI mice. These mice were originally obtained from the RIKEN Brain Science Institute, Saitama, Japan, from Dr Takaomi C. Saido.[16] The mice were genotyped by Transnetyx using real-time polymerase chain reaction. For euthanasia, the mice were anesthetized with isoflurane followed by cervical dislocation and acute decapitation. Equal numbers of male and female mice were used for all experiments.

Levetiracetam Injections and Brain Collection

Levetiracetam (United States Pharmacopeial) was dissolved in sterile saline solution (0.9% sodium chloride). Equal numbers of male and female mice were randomly assigned to vehicle (VEH) or treatment groups and were given chronic intraperitoneal injections of saline solution of 75 mg/kg between 10 am and 1 pm each day for 30 consecutive days. At the end of the 30 day chronic treatment, the mice were anesthetized and transcardially perfused with cold phosphate-buffered saline (PBS). Brains were then hemisected with one-half for immunostaining and the other for biochemistry.

TMT-MS Sample Preparation

TMT-MS sample preparation was performed as previously described.[17] In brief, homogenized cortical brain extracts were prepared, and 200 μg of protein was used for TMT-MS sample preparation. Methanol-chloroform precipitation was used to separate proteins from lipids and impurities. The extracted protein was then resuspended in 6M guanidine in 100 mM *N*-(2-hydroxyethyl)piperazine-*N*′-ethanesulfonic acid (HEPES). The proteins were further processed via the reduction of disulfide bonds with dithiothreitol and alkylation of cysteine residues with iodoacetamide. Proteins were then digested for 3 h at room temperature (RT) with 1 μg of LysC (Promega) and then digested overnight at 37 °C with 2 μg of Trypsin. The digest was then acidified with formic acid and desalted using C18 HyperSep columns (ThermoFisher Scientific). The eluted peptide solution was dried before resuspension in 100 mM HEPES. Micro-BCA assay was subsequently performed to determine the concentration of peptides. 100 μg of peptide from each sample was then used for isobaric labeling. TMT 16-plex labeling was performed on peptide samples according to the manufacturer's instructions (ThermoFisher Scientific). After incubating for 75 min at room temperature, the reaction was quenched with 0.3% (v/v) hydroxylamine. Isobaric labeled samples were then combined 1:1:1:1:1:1:1:1:1:1:1:1:1:1:1:1 and subsequently desalted with C18 HyperSep columns. The combined isobaric labeled peptide samples were fractionated into eight fractions using high pH reversed-phase columns (Pierce). Peptide solutions were dried, stored at −80 °C, and reconstituted in liquid chromatography−mass spectrometry (LC−MS) buffer A (5% acetonitrile, 0.125% formic acid) for LC−-MS/MS analysis.

TMT-MS Analysis

TMT-MS analysis was performed as previously described.[17] In short, samples were resuspended in 20 μL of buffer A (5% acetonitrile, 0.125% formic acid), and micro-BCA was performed. 3 μg of each fraction was loaded for LC−MS analysis via an auto-sampler with a Thermo EASY nLC 100 UPLC pump onto a vented Pepmap100, 75 μm × 2 cm, nanoViper trap column coupled to a nanoViper analytical column (Thermo Scientific) with a stainless steel emitter tip assembled on the nanospray flex ion source with a spray voltage of 2000 V. Orbitrap Fusion was used to generate MS data. The chromatographic run was performed with a 4 h gradient beginning with 100% buffer A and 0% B and increased to 7% B over 5 min, then to 25% B over 160 min, 36% B over 40 min, 45% B over 10 min, 95% B over 10 min, and held at 95% B for 15 min before terminating the scan. Buffer A contained 5% acetonitrile (ACN) and 0.125% formic acid in H_2O, and buffer B contained 99.875 ACN with 0.125% formic acid. Multinotch MS3 method was programmed with the following parameters: ion transfer tube temp = 300 °C, easy-IC internal mass calibration, default charge state = 2, and cycle time = 3 s. MS1 detector was set to orbitrap with 60 K resolution, wide quad isolation, mass range = normal, scan range = 300−1800 m/z, max injection time = 50 ms, AGC target = 6×10^5, microscans = 1, RF lens = 60%, without source fragmentation, and datatype = positive and centroid.[17] Monoisotopic precursor selection was set to include charge states 2−7 and reject unassigned. Dynamic exclusion was allowed; $n = 1$ exclusion for 60 s with 10 ppm tolerance for high and low. The intensity threshold was set to 5×10^3. Precursor selection decision = most intense, top speed, 3 s. MS2 settings include isolation window = 0.7, scan range = auto normal, collision energy = 35% CID, scan rate = turbo, max injection time = 50 ms, AGC target = 6×10^5, and $Q = 0.25$. In MS3, the top 10 precursor peptides selected for analysis were then fragmented using 65% higher-energy collisional dissociation before orbitrap detection. A precursor selection range of 400−

https://doi.org/10.1021/acs.jproteome.1c00180
J. Proteome Res. 2021, 20, 3580−3589

1200 m/z was chosen with mass range tolerance. An exclusion mass width was set to 18 ppm on the low and 5 ppm on the high. Isobaric tag loss exclusion was set to TMT reagent. Additional MS3 settings include an isolation window = 2, orbitrap resolution = 60 K, scan range = 120−500 m/z, AGC target = 6×10^5, max injection time = 120 ms, microscans = 1, and datatype = profile.

TMT-MS Data Analysis and Quantification

TMT-MS data analysis was performed as previously described in ref 17. In short, protein identification, TMT quantification, and analysis were performed with The Integrated Proteomics Pipeline-IP2 (Integrated Proteomics Applications, Inc., http://www.integratedproteomics.com/). Proteomic results were analyzed with ProLuCID, DTASelect2, Census, and QuantCompare. MS1, MS2, and MS3 spectrum raw files were extracted using RawExtract 1.9.9 software (http://fields.scripps.edu/downloads.php). Pooled spectral files from all eight fractions for each sample were then searched against the Uniprot mouse protein database and matched to sequences using the ProLuCID/SEQUEST algorithm (ProLuCID ver. 3.1) with 50 ppm peptide mass tolerance for precursor ions and 600 ppm for fragment ions. Fully and half-tryptic peptide candidates were included in the search space, all that fell within the mass tolerance window with no miscleavage constraint, assembled, and filtered with DTASelect2 (ver. 2.1.3) through the Integrated Proteomics Pipeline (IP2 v.5.0.1, Integrated Proteomics Applications, Inc., CA, USA). Static modifications at 57.02146 C and 304.2071 K and N-term were included. The target-decoy strategy was used to verify peptide probabilities and false discovery ratios.[18] A minimum peptide length of five was set for the process of each protein identification, and each dataset included a 1% FDR rate at the protein level based on the target-decoy strategy. Isobaric labeling analysis was established with Census 2 as previously described. TMT channels were normalized by dividing it over the sum of all channels.[18] No intensity threshold was applied. The fold change was then calculated as the mean of the experimental group standardized values, and p-values were then calculated by Student's t-test with Benjamini-Hochberg adjustment.

Online Databases for PANTHER and STRING (http://string-db.org)

Protein ontologies were determined with protein analysis through evolutionary relationship (PANTHER) system (http://www.pantherdb.org) in complete cellular component categories.[19] The statistical overrepresentation test was calculated by using the significant proteins identified from comparing VEH versus levetiracetam experimental groups for each *App* KI genotype as the query and the aggregated total proteins identified in all three comparisons as the reference. Protein ontologies with Fisher statistical tests with false discovery rate correction less than 0.05 were considered significant.

The search tool for the retrieval of interacting genes (STRING) database was used to determine protein−protein interactions from significant quantified proteins identified by the gene ontology cell component (GO:CC) term. The STRING resource is available at http://string-db.org.[20] The corresponding protein−protein interaction networks were constructed with the highest confidence of interaction score at 0.9.

Thioflavin Staining

After transcardial perfusion with cold PBS, hemisected brains were drop fixed in 4% paraformaldehyde overnight, cryoprotected in 30% sucrose for 2 days, embedded in a cryomold with OCT, flash frozen on dry ice, and stored at −80 °C until cryosectioning. 30 μm sagittal cryosections were prepared and mounted onto gelatin-coated slides (SouthernBiotech). Sections were then prepared for thioflavin S staining following standard procedures.[21] In short, the sections were washed with 70% ethanol for 1 min followed by 80% ethanol for 1 min before being incubated in filtered thioflavin S solution (1% in 80% ethanol) for 15 min in the dark. Slides were then washed sequentially with 80% ethanol, then 70% ethanol, and then distilled water for 1 min each. Coverslips were mounted using Fluoromount-G (SouthernBiotech). Sections were imaged at the Northwestern University Center for Advanced Microscopy with a TissueGnostics system using a 10× objective. Analysis was conducted using Fiji with the analyze puncta tool following thresholding. Cortical area analyzed was kept consistent throughout each section.

$A\beta_{42}$ ELISA Assay

$A\beta_{42}$ levels were measured using a human $A\beta_{42}$ ELISA kit (Thermo Scientific) following manufacturer instructions. In short, 5M guanidine HCl was added to cortical homogenates (1−2 mg) and kept shaking for 1 h at RT. Samples were then diluted 1:10 for $App^{NL/NL}$ and $App^{NL\text{-}F/NL\text{-}F}$ and 1:1000 for $App^{NL\text{-}G\text{-}F/NL\text{-}G\text{-}F}$ in standard diluent buffer. 50 μL of sample was loaded into wells coated with the provided $A\beta_{42}$ antibody and incubated for 3 h at RT. After three washes, horseradish peroxidase-conjugated antibody was added for 30 min. After another wash step, the samples were incubated with stabilized chromogen for 30 min, and the reaction was stopped with an acid-based stop solution. Finally, OD was measured at 450 nm using a Synergy HTX multimode microplate reader (Biotek) and compared to a standard curve to determine the final concentration.

Western Blotting

Cortical brain extracts were homogenized in 500 μL of homogenization buffer (4 mM HEPES, 0.32 M sucrose, 0.1 mM $MgCl_2$) supplemented with a protease inhibitor cocktail (aprotinin, leupeptin, AEBSF, benzamidine, PMSF, and pepstatin A). The tissue was then homogenized using a bead-based Precellys homogenizer. Protein concentration was then determined by BCA assay (Thermo Scientific) as per manufacturer's instructions and compared with the respective standard curve. 50 μg of each sample was then prepared for western blots (WB) by adding 6× sodium dodecyl sulfate sample buffer. The mixtures were sonicated and boiled at 96 °C for 5 min each and then loaded in 16% Tris-glycine gel. Gels were run at 80 V for 4 h and then wet transferred to a 0.2 μm nitrocellulose membrane. Membranes were then blocked with Odyssey Blocking Buffer (LI-COR) in PBS for 1 h and then incubated overnight with anti-amyloid beta precursor protein (Y188) rabbit monoclonal antibody at 1:1,000 (Abcam Cat# ab32136) and anti-VCP mouse monoclonal antibody at 1:2000 (Abcam Cat# ab11433). Next day, the membranes were washed and incubated in secondary antibody IRDye 800CW Donkey anti-Rabbit IgG antibody (LI-COR Biosciences Cat# 926-32213) and IRDye 680RD Donkey anti-Mouse IgG antibody (LI-COR Biosciences Cat# 925-68072) for 1 h at RT. Blots were imaged on an Odyssey CLx (LI-COR).

https://doi.org/10.1021/acs.jproteome.1c00180
J. Proteome Res. 2021, 20, 3580−3589

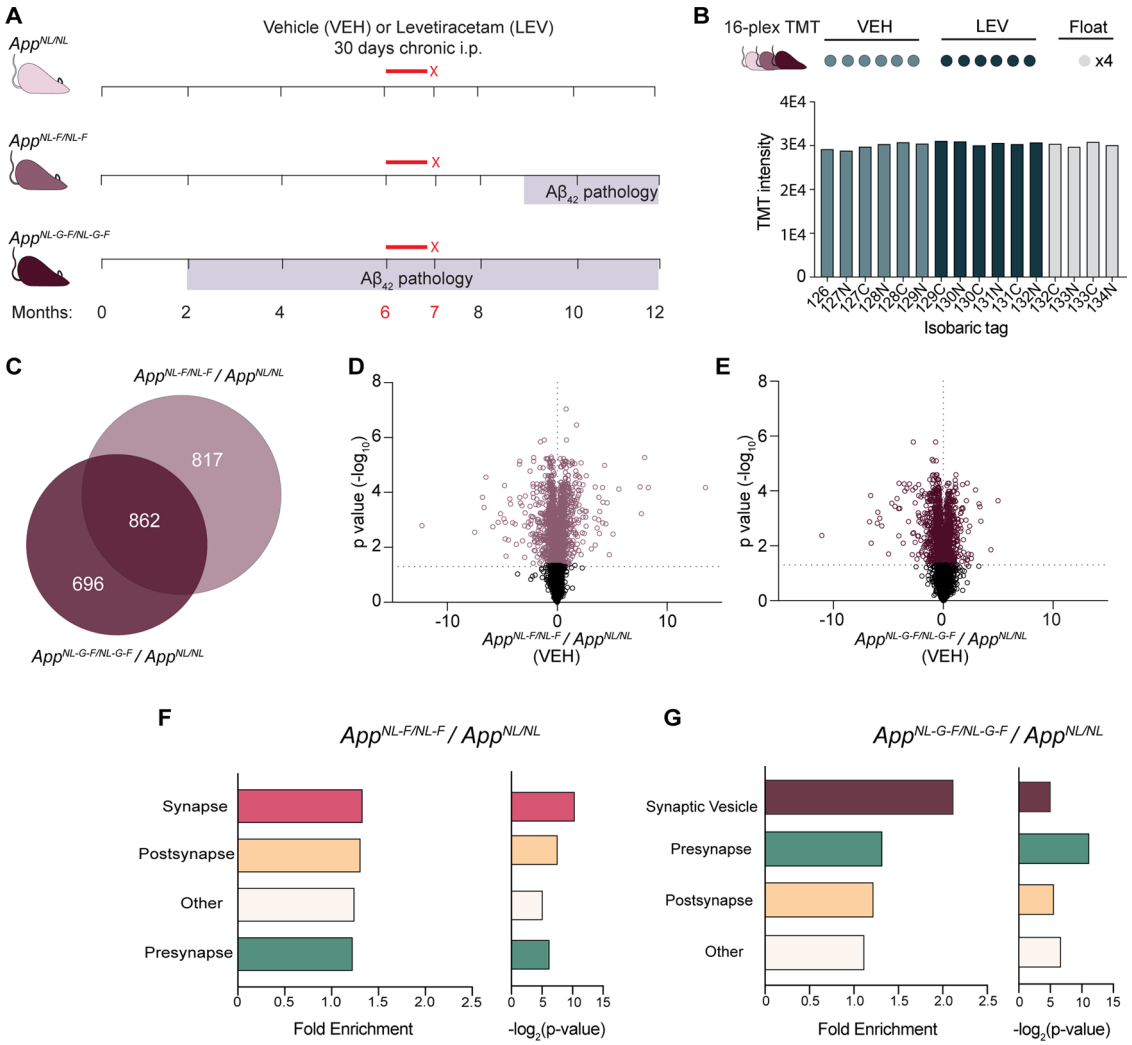

Figure 1. SV machinery proteins have selective and significantly altered fold change in $App^{NL\text{-}F/NL\text{-}F}$ and $App^{NL\text{-}G\text{-}F/NL\text{-}G\text{-}F}$ compared to $App^{NL/NL}$ cortical extracts. (A) Schematic depicting drug injections in relation to the onset of $A\beta_{42}$ pathology in $App^{NL/NL}$, $App^{NL\text{-}F/NL\text{-}F}$, and $App^{NL\text{-}G\text{-}F/NL\text{-}G\text{-}F}$ genotypes. Mice from each *App KI* genotype was VEH ($N = 6$) or levetiracetam treated ($N = 6$). (B) Schematic depicting the 16-plex TMT-MS experimental design. Each genotype $App^{NL/NL}$, $App^{NL\text{-}F/NL\text{-}F}$, and $App^{NL\text{-}G\text{-}F/NL\text{-}G\text{-}F}$ was analyzed in a 16-plex TMT-MS experiment comparing VEH to LEV treatments with four float channels for data normalization between experiments. Representative overall TMT channel peak intensities for each isobaric tag from the $App^{NL\text{-}G\text{-}F/NL\text{-}G\text{-}F}$ 16-plex TMT-MS experiment demonstrating equal labeling across all channels. (C) Venn diagram of significantly altered proteins (B.H. p-value < 0.05) between $App^{NL\text{-}F/NL\text{-}F}/App^{NL/NL}$ and $App^{NL\text{-}G\text{-}F/NL\text{-}G\text{-}F}/App^{NL/NL}$. Values indicate total number of significantly altered proteins. (D,E) Volcano plots depicting protein fold change for VEH $App^{NL\text{-}F/NL\text{-}F}$ compared to $App^{NL/NL}$ (D) and VEH $App^{NL\text{-}G\text{-}F/NL\text{-}G\text{-}F}$ compared to $App^{NL/NL}$ (E). Significant proteins (B.H. p-value < 0.05) are colored, and nonsignificant proteins are shown in gray (Table S1). (F,G) GO:CC enrichment analysis of significantly altered proteins in VEH $App^{NL\text{-}F/NL\text{-}F}/App^{NL/NL}$ (F) and VEH $App^{NL\text{-}G\text{-}F/NL\text{-}G\text{-}F}/App^{NL/NL}$ (G) (Table S2). Bar graphs depict fold enrichment of each significant GO term. $N = 6$ for each group. Data represents mean ± SEM analyzed with unpaired Student's t-test or one-way ANOVA with post hoc Sidak test. *p-value < 0.05, and **p-value < 0.01. LEV, levetiracetam.

Quantification and Statistical Analysis

Statistical analyses were performed using GraphPad Prism. All values in figures with error bars are presented as mean ± standard error of the mean (SEM). Comparison of VEH versus LEV groups was performed using unpaired Student's t-tests. Comparisons across all three genotypes were performed by one-way analysis of variance (ANOVA) and post hoc Fisher's test. P-values < 0.05 were considered statistically significant. Multiple test correction was performed with the Benjamini−Hochberg correction. For Bayesian analysis of variance, we implemented BAMarray 2.0, a Java software package that implements the Bayesian ANOVA for microarray (BAM) algorithm.[22] The BAM approach uses a special type of inferential regularization known as spike-and-slab shrinkage, which provides an optimal balance between total false detections (the total number of genes falsely identified as being differentially expressed) and total false nondetections (the total number of genes falsely identified as being nondifferentially expressed).[22]

RESULTS

SV-Associated Proteins Have Altered Abundance in $App^{NL\text{-}F/NL\text{-}F}$ and $App^{NL\text{-}G\text{-}F/NL\text{-}G\text{-}F}$ Cortical Extracts

We designed our experiments to investigate the effect of chronic levetiracetam in *App* KI brains with varying degrees of $A\beta_{42}$ pathology. The $App^{NL/NL}$ model serves as a relative control that does not develop $A\beta_{42}$ pathology, while $App^{NL\text{-}F/NL\text{-}F}$ mice have a relatively slow progressing $A\beta_{42}$ pathology. $App^{NL\text{-}G\text{-}F/NL\text{-}G\text{-}F}$ present with aggressive $A\beta_{42}$ pathology that is abundantly present by 6 months of age (Figure 1a). Levetiracetam at 75 mg/

https://doi.org/10.1021/acs.jproteome.1c00180
J. Proteome Res. 2021, 20, 3580−3589

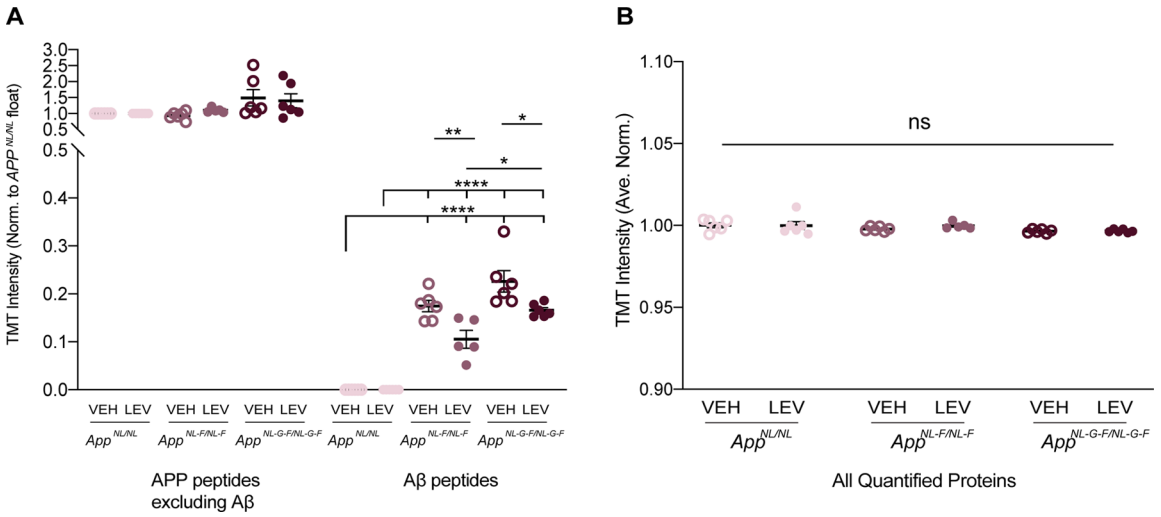

Figure 2. Chronic levetiracetam administration selectively lowers levels of $A\beta_{42}$ in $App^{NL\text{-}G\text{-}F/NL\text{-}G\text{-}F}$ cortex. (A) Normalized TMT intensities relative to $App^{NL/NL}$ of APP peptides mapping outside or within the $A\beta_{42}$ sequence comparing VEH and LEV groups of $App^{NL/NL}$, $App^{NL\text{-}F/NL\text{-}F}$, and $App^{NL\text{-}G\text{-}F/NL\text{-}G\text{-}F}$ animals. Aβ amino acid sequences for each *App* KI genotype: $App^{NL/NL}$, L.DAEFRHDSGYEVHHQK.L; $App^{NL\text{-}F/NL\text{-}F}$, K.LVFFAEDVGSNK.G; $App^{NL\text{-}G\text{-}F/NL\text{-}G\text{-}F}$, K.LVFFAGDVGSNK.G. (B) Normalized global TMT intensities for all proteins in $App^{NL/NL}$, $App^{NL\text{-}F/NL\text{-}F}$, and $App^{NL\text{-}G\text{-}F/NL\text{-}G\text{-}F}$ VEH and LEV groups. Each circle represents an individual biological replicate. $N = 6$ for each group. Data represents mean ± SEM analyzed with unpaired Student's t-test or one-way ANOVA with post hoc Sidak test. *p-value < 0.005.*p-value < 0.05, **p-value < 0.01, and ***p-value < 0.001. LEV, levetiracetam.

kg or VEH saline solution was administered intraperitoneally daily for 30 days beginning at 6 months of age for each *App* KI model (Figure 1a). To investigate levetiracetam's mode of action, we performed a quantitative bottom-up proteomic screen using guanidine HCl soluble cortical extracts with 16-plex TMT-MS. We compared protein abundance between cohorts given VEH ($N = 6$) or levetiracetam ($N = 6$) of the same *App* KI genotype along with multiple float channels that allow for comparisons between the multiple TMT-MS experiments (i.e., genotypes).

The overall TMT channel peak intensities were similar in all three experiments, indicating efficient labeling (Figure 1b). To assess the reliability of the TMT-MS data, we plotted the number of total quantified proteins, reporter ion intensities, and fold change distribution and confirmed similar data quality (Figure S1a–d). We compared the protein abundance in VEH $App^{NL\text{-}F/NL\text{-}F}$ to $App^{NL/NL}$ cohorts and identified 1704 significantly altered proteins (Figure 1c–e; Table S1). In the parallel VEH $App^{NL\text{-}G\text{-}F/NL\text{-}G\text{-}F}$ dataset, we identified 1578 significantly altered proteins compared to $App^{NL/NL}$ (Figure 1c–e; Table S1). To mine the significantly regulated proteins in $App^{NL\text{-}F/NL\text{-}F}/App^{NL/NL}$ and $App^{NL\text{-}G\text{-}F/NL\text{-}G\text{-}F}/App^{NL/NL}$, we performed GO:CC enrichment analysis with PANTHER. In both datasets, the regulated proteins are significantly enriched for the GO:CC terms: SV, synapse, presynapse, postsynapse, and others (Figure 1f,g; Table S2). This is consistent with our previous report that $App^{NL\text{-}F/NL\text{-}F}$ and $App^{NL\text{-}G\text{-}F/NL\text{-}G\text{-}F}$ brains both have synaptic proteome alterations by 6 months of age.[8] These results confirm the reliability of our TMT-MS analyses and extend our previous findings that the axon terminal proteome represents an early site of amyloid pathology.

Chronic Levetiracetam Administration Normalizes Levels of Presynaptic Endocytic Proteins in $App^{NL\text{-}G\text{-}F/NL\text{-}G\text{-}F}$ Cortex

To investigate the effect of chronic levetiracetam on Aβ levels, we extracted the relative peptide abundance mapping either inside or outside the Aβ amino acid sequence within APP. We quantified differences relative to the $App^{NL/NL}$ bridge channel that allows for comparison in the levels of peptide mapping to APP or Aβ across multiple TMT-MS experiments. This allows for quantification of peptide abundance relative to APP levels. APP peptide mapping outside of Aβ showed significant differences when comparing all three *App* KI genotypes [$F(5,29) = 2.711$, p-value = 0.0396]; however, post hoc analysis showed no significant differences in abundance between any of the groups of all three *App* KI genotypes (Figure 2a). Peptide mapping to the Aβ amino acid sequence was quantified across the *App* KI genotypes and showed, as expected, that cortical extracts from $App^{NL/NL}$ cohorts had significantly lower Aβ levels compared to $App^{NL\text{-}F/NL\text{-}F}$ *and* $App^{N\text{-}G\text{-}FL/NL\text{-}G\text{-}F}$ cohorts (p-value = <0.0001). Notably, in cortical extracts from levetiracetam-treated $App^{NL\text{-}F/NL\text{-}F}$ and $App^{NL\text{-}G\text{-}F/NL\text{-}G\text{-}F}$ mice, peptide mapping to the Aβ amino acid sequence was significantly reduced compared to their respective VEH-treated controls (p-value = 0.0095, p-value = 0.0211) (Figure 2a). A single tryptic Aβ peptide was quantified in the $App^{NL\text{-}F/NL\text{-}F}$ TMT-MS analysis, and one Aβ peptide containing the artic mutation was quantified in three instances during the $App^{N\text{-}G\text{-}FL/NL\text{-}G\text{-}F}$ TMT-MS analysis. Overall, we found that chronic levetiracetam had no significant effect on global protein abundance [$F(5,29) = 1.719$, p-value = 0.1617] (Figure 2b). These findings indicate that levetiracetam treatment can lower steady-state Aβ levels without altering the overall APP levels in $App^{NL\text{-}F/NL\text{-}F}$ and $App^{NL\text{-}G\text{-}F/NL\text{-}G\text{-}F}$ mice. Importantly, levetiracetam treatment has the ability to lower Aβ levels in $App^{NL\text{-}G\text{-}F/NL\text{-}G\text{-}F}$ mice, which at 6 months of age already harbor robust Aβ pathology.

We next sought to investigate how levetiracetam affects the $App^{NL\text{-}G\text{-}F/NL\text{-}G\text{-}F}$ cortical proteome as we were primarily interested in investigating how it mitigates amyloid pathology in the brain. First, in order to investigate proteomic alterations resulting from levetiracetam treatment in the $App^{NL\text{-}G\text{-}F/NL\text{-}G\text{-}F}$ cortex, we performed a Bayesian analysis of variance.[22] This statistical technique is used for identification of differentially expressed genes or proteins using a unique type of signal-to-noise detection strategy that allows for the detection of less

https://doi.org/10.1021/acs.jproteome.1c00180
J. Proteome Res. 2021, 20, 3580−3589

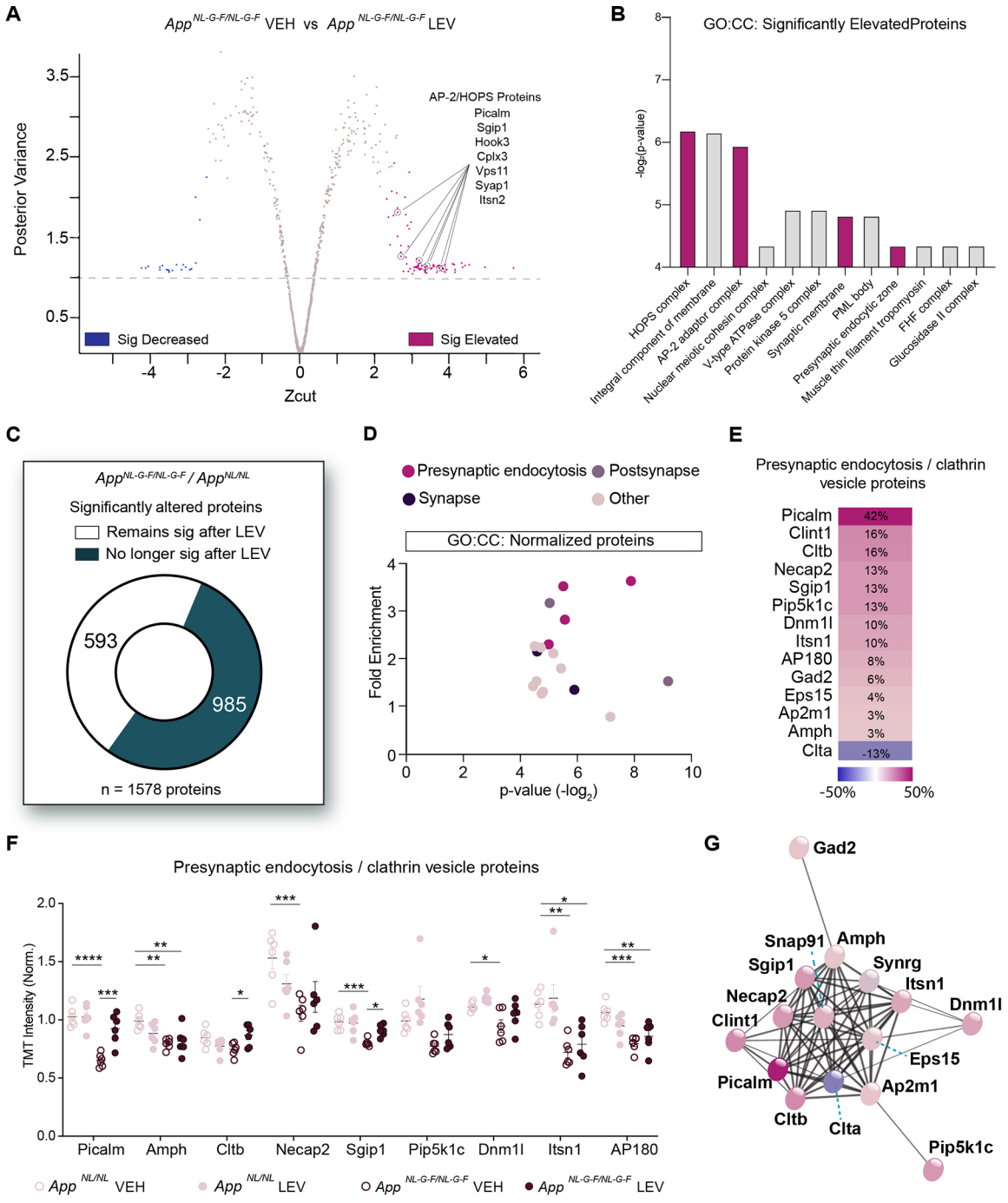

Figure 3. Chronic levetiracetam administration normalizes levels of presynaptic endocytic proteins in $App^{NL\text{-}G\text{-}F/NL\text{-}G\text{-}F}$ cortex. Presynaptic endocytic proteins are significantly upregulated with levetiracetam treatment in $App^{NL\text{-}G\text{-}F/NL\text{-}G\text{-}F}$. (A) Shrinkage plot from Bayesian analysis of variance showing proteins that are differentially expressed when directly comparing VEH and levetiracetam treatment in $App^{NL\text{-}G\text{-}F/NL\text{-}G\text{-}F}$ cohorts. Pink and blue dots indicated significantly elevated and decreased proteins, respectively. Gray dots indicate nonsignificant proteins. (B) GO:CC enrichment analysis of the panel of significantly upregulated proteins plots depict *p*-value ($-\log_2$) for each GO:CC term. Categories of high interest are indicated in pink. (C) Pie chart depicts significantly altered proteins identified by comparing VEH groups $App^{NL\text{-}G\text{-}F/NL\text{-}G\text{-}F}/App^{NL/NL}$. White indicates the number of proteins that remain significantly altered after LEV. Dark green denotes the proteins that no longer significantly altered after LEV (Table S3). (D) GO:CC enrichment analysis plots depict fold enrichment vs *p*-value ($-\log_2$) analyzed by Fisher's exact test. GO terms related to presynaptic endocytosis (pink), postsynapse (light purple), synapse (dark purple), and all other terms (light pink) (Table S4). (E) Percent change of presynaptic endocytosis proteins (GO:0098833) between VEH and LEV $App^{NL\text{-}G\text{-}F/NL\text{-}G\text{-}F}$ groups. (F) Normalized presynaptic endocytosis protein abundance between $App^{NL\text{-}G\text{-}F/NL\text{-}G\text{-}F}$ and $App^{NL/NL}$ VEH and LEV groups. (G) Protein−protein interaction hub of presynaptic endocytosis proteins based on STRING functional enrichment analysis. Data represents mean ± SEM analyzed with unpaired Student's t-test and BH correction. $N = 6$ per genotype, $N = 6$ per treatment group. Each circle represents an individual biological replicate. Data represents mean ± SEM analyzed with unpaired Student's t-test or one-way ANOVA with post-hoc Sidak test. *p-value < 0.005.*p-value < 0.05, **p-value <0 0.01, and ***p-value < 0.001. LEV, levetiracetam.

https://doi.org/10.1021/acs.jproteome.1c00180
J. Proteome Res. 2021, 20, 3580−3589

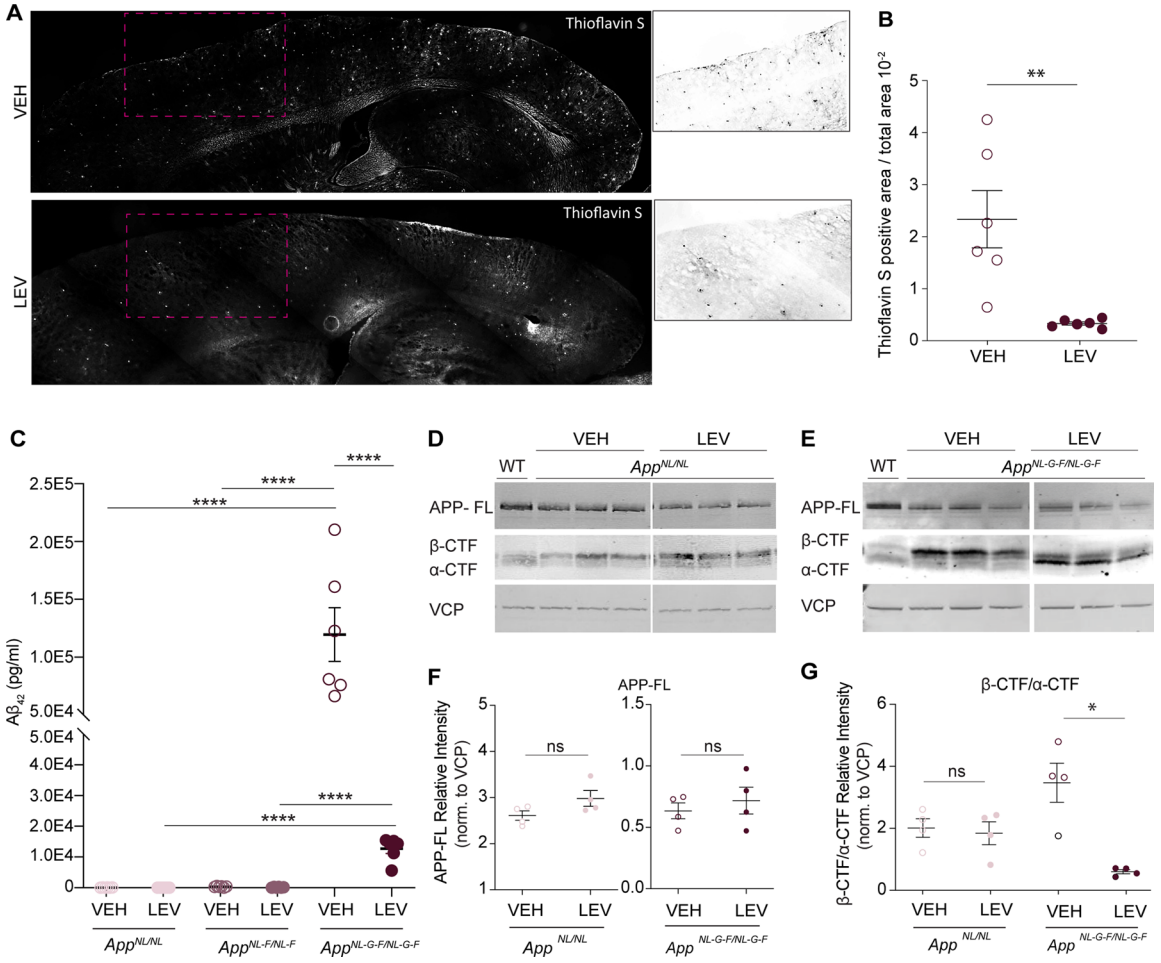

Figure 4. Chronic levetiracetam administration alters APP CTF production and decreases Aβ_{42} and in $App^{NL\text{-}G\text{-}F/NL\text{-}G\text{-}F}$. (A) Cortical amyloid pathology in $App^{NL\text{-}G\text{-}F/NL\text{-}G\text{-}F}$ comparing VEH and LEV treatment groups. Representative thioflavin S stained sagittal brain sections are shown. White box indicates area of magnified image. (B) Quantification of amyloid plaque puncta normalized to cortical area. (C) Aβ_{42} levels in cortical homogenates from $App^{NL/NL}$, $App^{NL\text{-}F/NL\text{-}F}$, and $App^{NL\text{-}G\text{-}F/NL\text{-}G\text{-}F}$ mice in VEH and LEV treated groups as measured by Aβ_{42} sandwich ELISA. $N = 6$ for each genotype and treatment group. Each circle represents an individual biological replicate. (D) Representative WB analysis of full-length APP and APP cleavage products, β-CTF, and α-CTF from cortical homogenates from $App^{NL/NL}$ VEH and LEV groups. Age-matched wild-type mouse age-matched cortical homogenates were used as a negative control. VCP was used to control loading and normalization. (E) Representative WB analysis of full-length APP and APP cleavage products, β-CTF, and α-CTF from cortical homogenates from $App^{NL\text{-}G\text{-}F/NL\text{-}G\text{-}F}$ groups. Age matched wild-type mouse cortical homogenates were used as a negative control. VCP was used to control loading. (F) Quantification of (D) showing the abundance of APP-FL normalized to VCP for $App^{NL/NL}$ and $App^{NL\text{-}G\text{-}F/NL\text{-}G\text{-}F}$ VEH and LEV groups. (G) Quantification of (E) showing the abundance of β-CTF/α-CTF ratio normalized to VCP. $N = 4$ for each genotype and treatment group. Each circle represents an individual biological replicate. Data represents mean ± SEM analyzed with unpaired Student's t-test or one-way ANOVA with post hoc Sidak test. *p-value < 0.05, **p-value < 0.01, and ***p-value < 0.001. LEV, levetiracetam.

robust yet significant signals in large datasets.[22] This allowed us to reveal proteins in the $App^{NL\text{-}G\text{-}F/NL\text{-}G\text{-}F}$ mice that were significantly elevated or reduced by levetiracetam treatment (Figure 3a). Proteins that were identified as significantly elevated with levetiracetam treatment were subjected to GO:CC enrichment analysis (Figure 3b). This showed that GO:CC terms related to presynaptic endocytosis (e.g., HOPS complex, AP-2 adaptor complex, presynaptic endocytic zone) were significantly upregulated by chronic levetiracetam.

In order to further probe how levetiracetam alters the proteome of $App^{NL\text{-}G\text{-}F/NL\text{-}G\text{-}F}$ animals, we honed in on the proteins that were significantly altered between the VEH-treated cohorts of $App^{NL\text{-}G\text{-}F/NL\text{-}G\text{-}F}$ and $App^{NL/NL}$. Next, we probed proteins from this comparison that were normalized by levetiracetam treatment (i.e., genotype vs drug effect).[23] Of the 1,578 significantly altered proteins in VEH $App^{NL\text{-}G\text{-}F/NL\text{-}G\text{-}F}$/$App^{NL/NL}$, 985 of those proteins were no longer significantly altered in the levetiracetam $App^{NL\text{-}G\text{-}F/NL\text{-}G\text{-}F}$/$App^{NL/NL}$ comparison, indicating that their levels were selectively modulated (Figure 3c; Table S3). We then performed GO:CC enrichment analysis of the 985 proteins with PANTHER and found again that the normalized proteins are most significantly enriched for GO:CC terms: presynaptic endocytosis, postsynapse, and synapse, among others (Figure 3d; Table S4). We then focused on the proteins belonging to the GO:CC term presynaptic endocytosis as this term was significant in both methods of analysis and investigated how their levels changed with treatment by comparing VEH to levetiracetam datasets for $App^{NL\text{-}G\text{-}F/NL\text{-}G\text{-}F}$. Notably, nearly all of the presynaptic endocytosis proteins had elevated levels after levetiracetam treatment (Figure 3e). We found that levetiracetam treatment in $App^{NL\text{-}G\text{-}F/NL\text{-}G\text{-}F}$ normalized presynaptic endocytosis protein levels back toward $App^{NL/NL}$ control levels (Figure 3f). To investigate the possibility that the levetiracetam-modulated

https://doi.org/10.1021/acs.jproteome.1c00180
J. Proteome Res. 2021, 20, 3580−3589

proteins physically interact, we subjected the group of normalized proteins to STRING analysis and uncovered a robust protein−protein interaction hub (Figure 3g). These regulated endocytic factors participate in all three predominant steps (i.e., initiation, assembly, and fission), suggesting that the entire process of endocytosis is modulated by levetiracetam (Figure S2a). At the 6 month time point, $App^{NL\text{-}F/NL\text{-}F}$ animals do not have significant Aβ_{42} pathology or plaque burden and therefore serve as an additional negative control. We performed parallel analyses for the $App^{NL\text{-}F/NL\text{-}F}$ datasets and found no synapse-associated proteomic alterations as a result of levetiracetam treatment (Figure S2b−e and Tables S3 and S4).

Levetiracetam Restores Nonamyloidogenic APP Processing in $App^{NL\text{-}G\text{-}F/NL\text{-}G\text{-}F}$ and Decreases Aβ_{42} Levels

To further investigate the effect of levetiracetam treatment on amyloid deposition, we performed thioflavin S staining on *App* KI sagittal sections. Quantification of thioflavin S puncta revealed that the treatment significantly decreased the amyloid plaque load in $App^{NL\text{-}G\text{-}F/NL\text{-}G\text{-}F}$ cortex compared to VEH treatment (p-value = 0.0046) (Figure 4a,b). In line with previous literature, VEH-treated $App^{NL\text{-}G\text{-}F/NL\text{-}G\text{-}F}$ mice had significantly more Aβ_{42} compared to VEH $App^{NL/NL}$ and $App^{NL\text{-}F/NL\text{-}F}$ mice based on sandwich ELISA (p-value = <0.0001; p-value = <0.0001) (Figure 4c). Interestingly, Aβ_{42} ELISA analysis revealed that levetiracetam-treated $App^{NL\text{-}G\text{-}F/NL\text{-}G\text{-}F}$ cortical extracts have significantly reduced Aβ_{42} levels (p-value = 0.0010) compared to VEH-treated $App^{NL\text{-}G\text{-}F/NL\text{-}G\text{-}F}$ cortical extracts (Figure 4c). Since Aβ_{42} levels are reduced without altering the levels of full-length APP protein, we investigated if the levels of APP cleavage products, β-CTF. and α-CTF were altered by levetiracetam. WB analysis of β-CTF and α-CTF bands from cortical homogenates were quantified in both $App^{NL/NL}$ and $App^{NL\text{-}G\text{-}F/NL\text{-}G\text{-}F}$ VEH and levetiracetam groups (Figures 4d−g and S3). Notably, analysis of the β-CTF/α-CTFs ratio from $App^{NL\text{-}G\text{-}F/NL\text{-}G\text{-}F}$ mice indicated that levetiracetam significantly decreases β-CTFs and correspondingly increases α-CTFs compared to VEH controls (p-value = 0.0010) (Figure 4g). There was no significant difference between the β-CTF/α-CTF ratio in the two $App^{NL/NL}$ groups. Importantly, in both $App^{NL/NL}$ and $App^{NL\text{-}G\text{-}F/NL\text{-}G\text{-}F}$, full-length APP showed no change in abundance (p-value = 0.1117; p-value = 0.5334) with levetiracetam treatment (Figure 4f). This finding suggests that chronic levetiracetam administration shifts APP processing toward the nonamyloidogenic pathway, which in turn limits Aβ_{42} production.

DISCUSSION

Taken all together, our work shows that chronic levetiracetam treatment in *App* KI mouse models normalizes levels of presynaptic endocytosis machinery and alters APP proteolytic processing corresponding with lower levels of Aβ_{42} and decreased amyloid plaque deposits. Using guanidine HCl-soluble cortical extracts from *App* KI mouse models, we were able to develop a profound understanding of the proteomic alterations that chronic levetiracetam treatment has on brains with varying stages of amyloid pathology. We note that while guanidine HCl extracts will contain both soluble and insoluble pools, it is possible that the varying abundance of insoluble proteins may affect our TMT-MS experiments. As a growing body of evidence has demonstrated an association between AD and brain hyperexcitability, understanding the relationship between neural network dysfunction and Aβ pathology is crucial.[6,14,24,25] Interestingly, in a study of AD patients with epilepsy, a comparison of levetiracetam versus typical epilepsy drugs, lamotrigine and phenobarbital, demonstrated that while all drugs were equally effective in reducing seizures, only levetiracetam treatment led to improved performance on cognitive tasks.[26] Furthermore, in AD mouse models of APP overexpression such as APP/PS1 and hAPP J20, only levetiracetam reduced hyperexcitability while also decreasing Aβ plaque burden and cognitive deficits.[9−12] These findings suggest that while hyperactivity contributes to increased Aβ pathology, treating hyperactivity alone is not sufficient to alleviate AD pathology. Our lab recently identified an impairment in the turnover of SV-associated proteins at early stages of AD pathology. In this study, we hypothesized that levetiracetam's unique beneficial effect on AD pathology could result from the atypical nature of this antiepileptic targeting the presynaptic SV2A protein.[8] This work shows for the first time the proteomic alterations that result from chronic levetiracetam treatment in an AD mouse model without the caveat of APP overexpression and provides a potential mechanism of action for the documented therapeutic effect of levetiracetam. Our findings demonstrate that chronic levetiracetam treatment selectively normalizes levels of presynaptic endocytosis proteins and is capable of lowering Aβ_{42} levels by altering APP processing.

Several supporting lines of evidence implicate dysregulation of endocytosis and presynaptic endocytic proteins in AD, thus supporting why normalization of this process reduces amyloidogenic APP processing and ultimately Aβ_{42} production. Much of the previous evidence gathered on Aβ toxicity implicates the postsynaptic membrane as the primary site of toxicity.[27−30] However, the localization and processing of APP mainly occurs at presynaptic terminals, and it has been previously shown that APP interacts with SVs.[31,32] Additionally, genome-wide association studies over the last decade have identified several AD-associated variants of endocytosis-related genes including PICALM, BIN1, and SORL1.[33−35] PICALM, which is a recruiter of adaptor complex 2 (AP-2) and is required for clathrin-mediated endocytosis, was the most significantly modulated protein in our datasets. How modulation of PICALM affects APP processing is not well understood. Some evidence supports an inverse relationship between PICALM levels and Aβ_{42} pathology. For example, $APP^{sw/0}$ × $PICALM^{+/-}$ mice displayed hippocampal and cortical Aβ loads 4-fold higher compared to $APP^{sw/0}$ × $PICALM^{+/+}$ controls.[36] In addition, it has been shown that AP-2 is required for APP endocytosis and has the ability to alter APP processing by promoting BACE1 trafficking.[37] These studies proposed that AP-2 functions at the presynapse to sort BACE1, leading to a regulation of its degradation during neuronal activity.[37] This would explain why rescuing levels of endocytosis proteins, such as PICALM and AP-2, could result in a shift toward the nonamyloidogenic pathway of APP cleavage. Furthermore, additional proteins functioning in endocytosis, that were also normalized in our datasets, showed reduced levels in postmortem AD brains (e.g., AP180 and Dynamin1).[38,39] Taken all together, there is substantial evidence that suggests that endocytosis and intracellular sorting determines how APP is processed. As we have previously identified an Aβ-dependent impairment in degradation at axon terminals, we propose that an upregulation in endocytosis could be beneficial as it could boost impaired SV cycling, leading to removal of APP from membranes where it is

https://doi.org/10.1021/acs.jproteome.1c00180
J. Proteome Res. 2021, 20, 3580−3589

susceptible to secretase cleavage. Our data supports the concept that levetiracetam lowers $A\beta_{42}$ levels by normalizing the abundance of presynaptic endocytosis machinery that corresponds to a shift in APP processing toward the non-amyloidogenic pathway.

■ ASSOCIATED CONTENT

Supporting Information

The Supporting Information is available free of charge at https://pubs.acs.org/doi/10.1021/acs.jproteome.1c00180.

Table S1. Summary of relative abundances for significantly deferentially regulated proteins across *APP* KI genotypes from cortical extracts. Related to Figure 1 Table S2. Significantly over-represented cellular components from a GO analysis using the query of proteins that were significantly deferentially regulated in each data set against the reference of all proteins identified. Related to Figure 1 Table S3. Summary of significantly altered proteins identified by comparing vehicle groups $App^{NL\text{-}G\text{-}F/NL\text{-}G\text{-}F}/App^{NL/NL}$ or $App^{NL\text{-}F/LN\text{-}F}/App^{NL/NL}$ and the proteins that either remain or no longer are significantly altered after LEV. Related to Figure 3 and Figure S2 Table S4. Significantly over-represented cellular components from a GO analysis using the query of proteins that were no longer significantly deferentially regulated after LEV against the reference of all proteins identified. Related to Figure 3 and Figure S2 (PDF)

Figure S1. TMT-MS experiments have similar data quality (XLSX)

Figure S2. Differentially regulated proteins in $App^{NL\text{-}F/NL\text{-}F}$ levetiracetam versus vehicle cohorts (XLSX)

Figure S3. Chronic levetiracetam administration alters APP CTF production in $App^{NL\text{-}G\text{-}F/NL\text{-}G\text{-}F}$ (XLSX)

Western blot full images related to Figure 4 (XLSX)

■ AUTHOR INFORMATION

Corresponding Author

Jeffrey N. Savas − *Department of Neurology, Northwestern University Feinberg School of Medicine, Chicago, Illinois 60611, United States;* orcid.org/0000-0001-6727-2439; Email: jeffrey.savas@northwestern.edu

Author

Nalini R. Rao − *Department of Neurology, Northwestern University Feinberg School of Medicine, Chicago, Illinois 60611, United States*

Complete contact information is available at: https://pubs.acs.org/10.1021/acs.jproteome.1c00180

Author Contributions

N.R.R. and J.N.S. designed the experiments; N.R.R. performed all experiments; and N.R.R. and J.N.S. wrote the manuscript. All authors read and approved the final manuscript.

Funding

This work was supported by the NIH, R01AG061787, R01AG061865, and R21NS107761 to J.N.S; N.R.R. is supported by Mechanisms of Aging and Dementia T32AG20506 as well as the Cure Alzheimer's Fund and a pilot award from the CNADC of Northwestern Medicine to J.N.S.

Notes

The authors declare no competing financial interest.

Further information and requests for resources and reagents should be directed to and will be fulfilled by the Lead Contact, Jeffrey N Savas (jeffrey.savas@northwestern.edu). The raw MS data have been deposited in MassIVE online database (MSV000087285) (https://massive.ucsd.edu/ProteoSAFe/static/massive.jsp) and upon acceptance will be available in the ProteomeXchange online database (http://www.proteomexchange.org/).

■ ACKNOWLEDGMENTS

We thank Tim Hark for contributing to thioflavin S imaging and tissue collection. We thank the NU Center for Advanced Microscopy, which is generously supported by NCI CCSG P30 CA060553 awarded to the Robert H. Lurie Comprehensive Cancer Center.

■ ABBREVIATIONS

Aβ, amyloid-beta; APP, amyloid precursor protein; AD, Alzheimer's disease; *App* KI, APP knock-in; β-CTF/α-CTF, beta/alpha carboxyl-terminal fragment; GO, gene ontology; LEV, levetiracetam; MS, mass spectrometry; SV, synaptic vesicle; SV2A, synaptic vesicle glycoprotein 2A; TMT, tandem mass tag; VEH, vehicle

■ REFERENCES

(1) Zhou, Y.; Zhao, Y.; Xie, H.; Wang, Y.; Liu, L.; Yan, X. Alteration in amyloid β42, phosphorylated tau protein, interleukin 6, and acetylcholine during diabetes-accelerated memory dysfunction in diabetic rats: correlation of amyloid β42 with changes in glucose metabolism. *Behav. Brain Funct.* **2015**, *11*, 24.

(2) Lacor, P. N.; Buniel, M. C.; Furlow, P. W.; Clemente, A. S.; Velasco, P. T.; Wood, M.; Viola, K. L.; Klein, W. L. Aβ Oligomer-Induced Aberrations in Synapse Composition, Shape, and Density Provide a Molecular Basis for Loss of Connectivity in Alzheimer's Disease. *J. Neurosci.* **2007**, *27*, 796−807.

(3) Lambert, M. P.; Barlow, A. K.; Chromy, B. A.; Edwards, C.; Freed, R.; Liosatos, M.; Morgan, T. E.; Rozovsky, I.; Trommer, B.; Viola, K. L.; Wals, P.; Zhang, C.; Finch, C. E.; Krafft, G. A.; Klein, W. L. Diffusible, nonfibrillar ligands derived from Aβ1−42 are potent central nervous system neurotoxins. *Proc. Natl. Acad. Sci. U.S.A.* **1998**, *95*, 6448−6453.

(4) Herrup, K. The case for rejecting the amyloid cascade hypothesis. *Nat. Neurosci.* **2015**, *18*, 794−799.

(5) Palop, J. J.; Mucke, L. Epilepsy and cognitive impairments in alzheimer disease. *Arch. Neurol.* **2009**, *66*, 435−440.

(6) Kuchibhotla, K. V.; Goldman, S. T.; Lattarulo, C. R.; Wu, H.-Y.; Hyman, B. T.; Bacskai, B. J. Abeta plaques lead to aberrant regulation of calcium homeostasis in vivo resulting in structural and functional disruption of neuronal networks. *Neuron* **2008**, *59*, 214−225.

(7) Palop, J. J.; Chin, J.; Roberson, E. D.; Wang, J.; Thwin, M. T.; Bien-Ly, N.; Yoo, J.; Ho, K. O.; Yu, G.-Q.; Kreitzer, A.; Finkbeiner, S.; Noebels, J. L.; Mucke, L. Aberrant excitatory neuronal activity and compensatory remodeling of inhibitory hippocampal circuits in mouse models of Alzheimer's disease. *Neuron* **2007**, *55*, 697−711.

(8) Hark, T. J.; Rao, N. R.; Castillon, C.; Basta, T.; Smukowski, S.; Bao, H.; Savas, J. N. Pulse-chase proteomics of the App Knockin mouse models of Alzheimer's disease reveals that synaptic dysfunction originates in presynaptic terminals. *Cell Syst.* **2020**, *12*, 141−158.

(9) Vossel, K. A.; Tartaglia, M. C.; Nygaard, H. B.; Zeman, A. Z.; Miller, B. L. Epileptic activity in Alzheimer's disease: causes and clinical relevance. *Lancet Neurol.* **2017**, *16*, 311−322.

(10) Sanchez, P. E.; Zhu, L.; Verret, L.; Vossel, K. A.; Orr, A. G.; Cirrito, J. R.; Devidze, N.; Ho, K.; Yu, G.-Q.; Palop, J. J.; Mucke, L. Levetiracetam suppresses neuronal network dysfunction and reverses

synaptic and cognitive deficits in an Alzheimer's disease model. *Proc. Natl. Acad. Sci. U.S.A.* **2012**, *109*, E2895−E2903.
(11) Shi, J.-Q.; Wang, B.-R.; Tian, Y.-Y.; Xu, J.; Gao, L.; Zhao, S.-L.; Jiang, T.; Xie, H.-G.; Zhang, Y.-D. Antiepileptics topiramate and levetiracetam alleviate behavioral deficits and reduce neuropathology in APPswe/PS1dE9 transgenic mice. *CNS Neurosci. Ther.* **2013**, *19*, 871−881.
(12) Koh, M. T.; Haberman, R. P.; Foti, S.; McCown, T. J.; Gallagher, M. Treatment strategies targeting excess hippocampal activity benefit aged rats with cognitive impairment. *Neuropsychopharmacology* **2010**, *35*, 1016−1025.
(13) Nygaard, H. B.; Kaufman, A. C.; Sekine-Konno, T.; Huh, L. L.; Going, H.; Feldman, S. J.; Kostylev, M. A.; Strittmatter, S. M. Brivaracetam, but not ethosuximide, reverses memory impairments in an Alzheimer's disease mouse model. *Alzheimer's Res. Ther.* **2015**, *7*, 25.
(14) Bakker, A.; Krauss, G. L.; Albert, M. S.; Speck, C. L.; Jones, L. R.; Stark, C. E.; Yassa, M. A.; Bassett, S. S.; Shelton, A. L.; Gallagher, M. Reduction of hippocampal hyperactivity improves cognition in amnestic mild cognitive impairment. *Neuron* **2012**, *74*, 467−474.
(15) Toniolo, S.; Sen, A.; Husain, M. Modulation of Brain Hyperexcitability: Potential New Therapeutic Approaches in Alzheimer's Disease. *Int. J. Mol. Sci.* **2020**, *21*, 9318.
(16) Saito, T.; Matsuba, Y.; Mihira, N.; Takano, J.; Nilsson, P.; Itohara, S.; Iwata, N.; Saido, T. C. Single App knock-in mouse models of Alzheimer's disease. *Nat. Neurosci.* **2014**, *17*, 661−663.
(17) Jongkamonwiwat, N.; Ramirez, M. A.; Edassery, S.; Wong, A. C. Y.; Yu, J.; Abbott, T.; Pak, K.; Ryan, A. F.; Savas, J. N. Noise Exposures Causing Hearing Loss Generate Proteotoxic Stress and Activate the Proteostasis Network. *Cell Rep.* **2020**, *33*, 108431.
(18) McAlister, G. C.; Nusinow, D. P.; Jedrychowski, M. P.; Wühr, M.; Huttlin, E. L.; Erickson, B. K.; Rad, R.; Haas, W.; Gygi, S. P. MultiNotch MS3 enables accurate, sensitive, and multiplexed detection of differential expression across cancer cell line proteomes. *Anal. Chem.* **2014**, *86*, 7150−7158.
(19) Mi, H.; Poudel, S.; Muruganujan, A.; Casagrande, J. T.; Thomas, P. D. PANTHER version 10: expanded protein families and functions, and analysis tools. *Nucleic Acids Res.* **2016**, *44*, D336−D342.
(20) Szklarczyk, D.; Morris, J. H.; Cook, H.; Kuhn, M.; Wyder, S.; Simonovic, M.; Santos, A.; Doncheva, N. T.; Roth, A.; Bork, P.; et al. The STRING database in 2017: quality-controlled protein-protein association networks, made broadly accessible. *Nucleic Acids Res.* **2017**, *45*, D362−D368.
(21) Ly, P. T. T.; Cai, F.; Song, W. Detection of neuritic plaques in Alzheimer's disease mouse model. *J. Visualized Exp.* **2011**, *53*, 2831.
(22) Ishwaran, H.; Rao, J. S. Detecting differentially expressed genes in microarrays using Bayesian model selection. *J. Am. Stat. Assoc.* **2003**, *98*, 438−455.
(23) He, Q.; Arroyo, E. D.; Smukowski, S. N.; Xu, J.; Piochon, C.; Savas, J. N.; Portera-Cailliau, C.; Contractor, A. Critical period inhibition of NKCC1 rectifies synapse plasticity in the somatosensory cortex and restores adult tactile response maps in fragile X mice. *Mol. Psychiatry* **2019**, *24*, 1732−1747.
(24) Harris, S. S.; Wolf, F.; De Strooper, B.; Busche, M. A. Tipping the Scales: Peptide-Dependent Dysregulation of Neural Circuit Dynamics in Alzheimer's Disease. *Neuron* **2020**, *107*, 417−435.
(25) Sen, A.; Capelli, V.; Husain, M. Cognition and dementia in older patients with epilepsy. *Brain* **2018**, *141*, 1592−1608.
(26) Cumbo, E.; Ligori, L. D. Levetiracetam, lamotrigine, and phenobarbital in patients with epileptic seizures and Alzheimer's disease. *Epilepsy Behav.* **2010**, *17*, 461−466.
(27) DeBoer, S. R.; Dolios, G.; Wang, R.; Sisodia, S. S. Differential release of beta-amyloid from dendrite- versus axon-targeted APP. *J. Neurosci.* **2014**, *34*, 12313−12327.
(28) Perdigão, C.; Barata, M. A.; Araújo, M. N.; Mirfakhar, F. S.; Castanheira, J.; Guimas Almeida, C. Intracellular trafficking mechanisms of synaptic dysfunction in Alzheimer's disease. *Front. Cell. Neurosci.* **2020**, *14*, 72.
(29) Serrano-Pozo, A.; Frosch, M. P.; Masliah, E.; Hyman, B. T. Neuropathological alterations in Alzheimer disease. *Cold Spring Harbor Perspect. Med.* **2011**, *1*, 006189.
(30) Sheng, M.; Sabatini, B. L.; Südhof, T. C. Synapses and Alzheimer's disease. *Cold Spring Harbor Perspect. Med.* **2012**, *4*, 005777.
(31) Masliah, E.; Honer, W. G.; Mallory, M.; Voigt, M.; Kushner, P.; Hansen, L.; Terry, R. Topographical distribution of synaptic-associated proteins in the neuritic plaques of Alzheimer's disease hippocampus. *Acta Neuropathol.* **1994**, *87*, 135−142.
(32) Oddo, S.; Caccamo, A.; Shepherd, J. D.; Murphy, M. P.; Golde, T. E.; Kayed, R.; Metherate, R.; Mattson, M. P.; Akbari, Y.; LaFerla, F. M. Triple-transgenic model of Alzheimer's disease with plaques and tangles: intracellular Abeta and synaptic dysfunction. *Neuron* **2003**, *39*, 409−421.
(33) Harold, D.; Abraham, R.; Hollingworth, P.; Sims, R.; Gerrish, A.; Hamshere, M. L.; Pahwa, J. S.; Moskvina, V.; Dowzell, K.; Williams, A.; et al. Genome-wide association study identifies variants at CLU and PICALM associated with Alzheimer's disease. *Nat. Genet.* **2009**, *41*, 1088−1093.
(34) Seshadri, S.; Fitzpatrick, A. L.; Ikram, M. A.; DeStefano, A. L.; Gudnason, V.; Boada, M.; Bis, J. C.; Smith, A. V.; Carassquillo, M. M.; Lambert, J. C.; et al. Genome-wide analysis of genetic loci associated with Alzheimer disease. *JAMA, J. Am. Med. Assoc.* **2010**, *303*, 1832−1840.
(35) Talwar, P.; Silla, Y.; Grover, S.; Gupta, M.; Agarwal, R.; Kushwaha, S.; Kukreti, R. Genomic convergence and network analysis approach to identify candidate genes in Alzheimer's disease. *BMC Genomics* **2014**, *15*, 199.
(36) Zhao, Z.; Sagare, A. P.; Ma, Q.; Halliday, M. R.; Kong, P.; Kisler, K.; et al. Central role for PICALM in amyloid-β blood-brain barrier transcytosis and clearance. *Nat. Neurosci.* **2015**, *18*, 978−987.
(37) Bera, S.; Camblor-Perujo, S.; Calleja Barca, E.; Negrete-Hurtado, A.; Racho, J.; De Bruyckere, E.; Wittich, C.; Ellrich, N.; Martins, S.; Adjaye, J.; Kononenko, N. L. AP-2 reduces amyloidogenesis by promoting BACE1 trafficking and degradation in neurons. *EMBO Rep.* **2020**, *21*, No. e47954.
(38) Yao, P. J.; Coleman, P. D. Reduction of O-linked N-acetylglucosamine-modified assembly protein-3 in Alzheimer's disease. *J. Neurosci.* **1998**, *18*, 2399−2411.
(39) Yao, P. J.; Zhu, M.; Pyun, E. I.; Brooks, A. I.; Therianos, S.; Meyers, V. E.; Coleman, P. D. Defects in expression of genes related to synaptic vesicle trafficking in frontal cortex of Alzheimer's disease. *Neurobiol. Dis.* **2003**, *12*, 97−109.

https://doi.org/10.1021/acs.jproteome.1c00180
J. Proteome Res. 2021, 20, 3580−3589